Coordination of protrusion dynamics within and between collectively migrating border cells by myosin II

Abhinava K. Mishra, James A. Mondo, Joseph P. Campanale, and Denise J. Montell*
Molecular, Cellular, and Developmental Biology Department, University of California, Santa Barbara, Santa Barbara, CA 93106

ABSTRACT **Collective cell migration is emerging as a major driver of embryonic development, organogenesis, tissue homeostasis, and tumor dissemination. In contrast to individually migrating cells, collectively migrating cells maintain cell–cell adhesions and coordinate direction-sensing as they move. While nonmuscle myosin II has been studied extensively in the context of cells migrating individually in vitro, its roles in cells migrating collectively in three-dimensional, native environments are not fully understood. Here we use genetics, Airyscan microscopy, live imaging, optogenetics, and Förster resonance energy transfer to probe the localization, dynamics, and functions of myosin II in migrating border cells of the *Drosophila* ovary. We find that myosin accumulates transiently at the base of protrusions, where it functions to retract them. E-cadherin and myosin colocalize at border cell-border cell contacts and cooperate to transmit directional information. A phosphomimetic form of myosin is sufficient to convert border cells to a round morphology and blebbing migration mode. Together these studies demonstrate that distinct and dynamic pools of myosin II regulate protrusion dynamics within and between collectively migrating cells and suggest a new model for the role of protrusions in collective direction sensing in vivo.**

Monitoring Editor
Carole Parent
University of Michigan

Received: Feb 26, 2019
Revised: Jul 22, 2019
Accepted: Jul 24, 2019

INTRODUCTION

Collective cell migration is essential for normal embryonic development and tissue homeostasis. It is also emerging as a major mechanism facilitating tumor metastasis (Friedl and Gilmour, 2009; Ewald *et al.*, 2012; Cheung *et al.*, 2013, 2016; Cheung and Ewald, 2014; Aceto *et al.*, 2014; Richardson *et al.*, 2018). Border cells in the *Drosophila* ovary provide an excellent model for studying fundamental mechanisms of collective cell migration in vivo (Friedl and Gilmour, 2009; Montell *et al.*, 2012). Border cells are a group of six to eight epithelial follicle cells that migrate roughly 150 microns in between large cells called nurse cells during stage 9 of oogenesis (Figure 1, A and B). The border cell cluster is composed of a central pair of nonmigratory polar cells, which secrete the cytokine Unpaired (Upd). Upd activates Jak/STAT signaling and motility in surrounding cells (Silver and Montell, 2001). Once specified, border cells round up and surround the polar cells. One or two border cells extend Rac-dependent protrusions between the nurse cells to initiate migration (Murphy and Montell, 1996; Fulga and Rørth, 2002; Prasad and Montell, 2007). Over the course of 3 to 6 h, the cluster migrates posteriorly toward the oocyte, arriving at the border by stage 10 (Figure 1C). There, they cooperate with other cells to form an eggshell structure called the micropyle (Montell *et al.*, 1992), which is the site of sperm entry. Thus, border cell migration is essential for fertility.

Some mechanisms of collective cell migration differ from those of single cells. For example, E-cadherin (Ecad) acts as a migration-suppressor in the context of the epithelial to mesenchymal transition (Onder *et al.*, 2008). However, the gene coding for E-cad, CDH1, is rarely deleted in human cancer (cbioportal.org). E-cad expression is maintained and required in collectively invasive mammary tumors (Rakha *et al.*, 2013; Shamir and Ewald, 2015;

This article was published online ahead of print in MBoC in Press (http://www.molbiolcell.org/cgi/doi/10.1091/mbc.E19-02-0124) on August 7, 2019.

*Address correspondence to: Denise J. Montell (dmontell@ucsb.edu).

Abbreviations used: ANOVA, analysis of variance; E-cad, E-cadherin; NA, numerical aperture; PA-Rac, photoactivatable-Rac; PBS, phosphate-buffered saline; PBST, phosphate-buffered saline containing 0.4% Triton X-100; RNAi, RNA interference; Sqh, Spaghetti squash; Upd, Unpaired; Zip, Zipper.

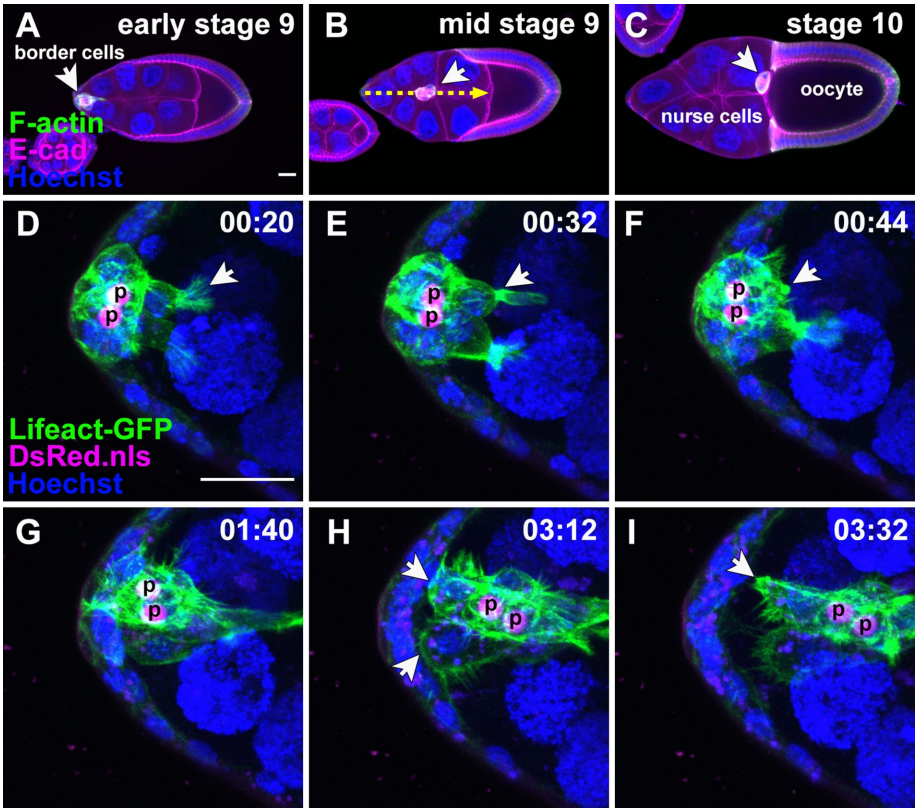

FIGURE 1: Distributions of E-cad and F-actin (labeled by phalloidin) before, during, and after border cell migration. (A–C) Maximum intensity projections of wild-type egg chambers labeled with E-cad (magenta), F-Actin (green), and Hoechst (blue) during stages 9 and 10 of *Drosophila* egg chamber development. (A) Border cells (white arrows) initiating migration. (B) Border cells in mid migration between nurse cells. Dashed yellow line indicates their migration path. (C) Border cells reach the oocyte border by stage 10. (D–I) Zoomed stills from time-lapse images of border expressing Lifeact-GFP driven by *slbo* regulatory sequences (green) and nuclear DsRed (UAS-DsRed.nls, magenta) driven by polar cell specific upd-Gal4. Polar cells marked with "p." Border cells (D–F) extend and retract protrusions (white arrows), prior to a single leader cell forming a dominant protrusion to lead the cluster in G–I delaminating from the anterior epithelium (white arrows). Numbers in G–I denote hours and minutes. All images are oriented anterior on the left and posterior on the right. Scale bars in A–C and D–I are the same. All scale bars are 20 μm.

Piotrowski-Daspit *et al.*, 2016). Therefore, understanding the positive roles of E-cad in collective cell migration can provide insights into the mechanisms of collective cell motility in both normal and disease contexts. However, there are relatively few models in which collectively migrating cells can be imaged live in their native environments and manipulated genetically and optogenetically. Border cells offer such a model.

During border cell migration, E-cad performs three essential functions (Niewiadomska *et al.*, 1999; Cai *et al.*, 2014). E-cad–mediated adhesion between polar cells and outer migratory cells maintains cluster cohesion and thus collective motility (Cai *et al.*, 2014), which is important because individual cells migrate less efficiently than clusters (Cai *et al.*, 2016). E-cad–mediated adhesion between the lead border cell and nurse cells participates in a positive feedback loop with guidance receptor signaling, the small GTPase Rac, and actin polymerization to generate the large leading protrusions that initiate and guide border cell migration. Finally, E-cad–mediated adhesion between individual border cells communicates direction from the leader to the following cells of the cluster to maintain coordinated movement (Wang *et al.*, 2010; Cai *et al.*, 2014). Mechanical coupling between leader and follower cells by classical cadherins has subsequently also been proposed for collectively invading tumor cells and tumor/stroma cell groups (Veracini *et al.*, 2015; Labernadie *et al.*, 2017).

The work by Cai *et al.* (2014) predicts that as the lead border cell protrudes and moves forward, it pulls on the following cells. Furthermore, the proposed model predicts that E-cad–mediated adhesions between border cells transmit force from cell to cell leading to inhibition of Rac activity in followers and thus reducing their probability of protrusion. One candidate for force transduction is the actomyosin cable that connects individual cells through cell–cell junctions. Therefore we set out to test the function of nonmuscle myosin II (hereafter myosin II) in communication of direction between border cells. Other roles for myosin in border cell migration have previously been described, including detachment of the cluster from the anterior end of the egg chamber (Majumder *et al.*, 2012) and maintenance of cluster morphology during migration (Aranjuez *et al.*, 2016). Here, we report previously unrecognized localizations and functions for myosin II during border cell migration. We use Airyscan microscopy, live imaging, RNA interference (RNAi), photoactivatable Rac, and a Förster resonance energy transfer (FRET)-based Rac activity sensor to probe the diverse and dynamic effects of myosin II on collective cell migration. We propose an integrated model for the multiple roles of dynamic myosin II activity in coordinating collective border cell migration.

RESULTS

Dynamic localization of myosin

Using confocal microscopy, we observed border cell migration live and at high spatiotemporal resolution during delamination (Figure 1; Supplemental Movie S1). The first morphological changes after border cell fate specification are that the cluster rounds up and multiple cells extend and retract actin-rich protrusions for ~1 h (Figure 1, D–F). Eventually a single leader cell with a dominant forward protrusion emerges (Figure 1G). As the lead cell moves forward, additional cells delaminate from the epithelium (Figure 1H), ultimately detaching from the epithelial cells that remain behind (Figure 1I).

Since myosin II assembles cooperatively on contractile filaments, accumulating to its highest levels at sites where it is active (Uehara *et al.*, 2010), we examined its localization together with F-actin during border cell migration. We used a fluorescently tagged form of myosin light chain, known in *Drosophila* as Spaghetti squash (Sqh). The Sqh-mCherry fusion protein is expressed under the endogenous genomic regulatory sequences and is fully functional (Martin *et al.*, 2009). Like E-cad (Cai *et al.*, 2014), Sqh-mCherry accumulates to higher levels in somatic cells than in the germline (Figure 2, A–D) even though the germline contains high levels of F-actin (Figure 2, A and B). The Sqh-mCherry protein is present in border cells throughout their migration and is enriched near the apical surfaces of all follicle cells (Figure 2, A–D) including polar cells

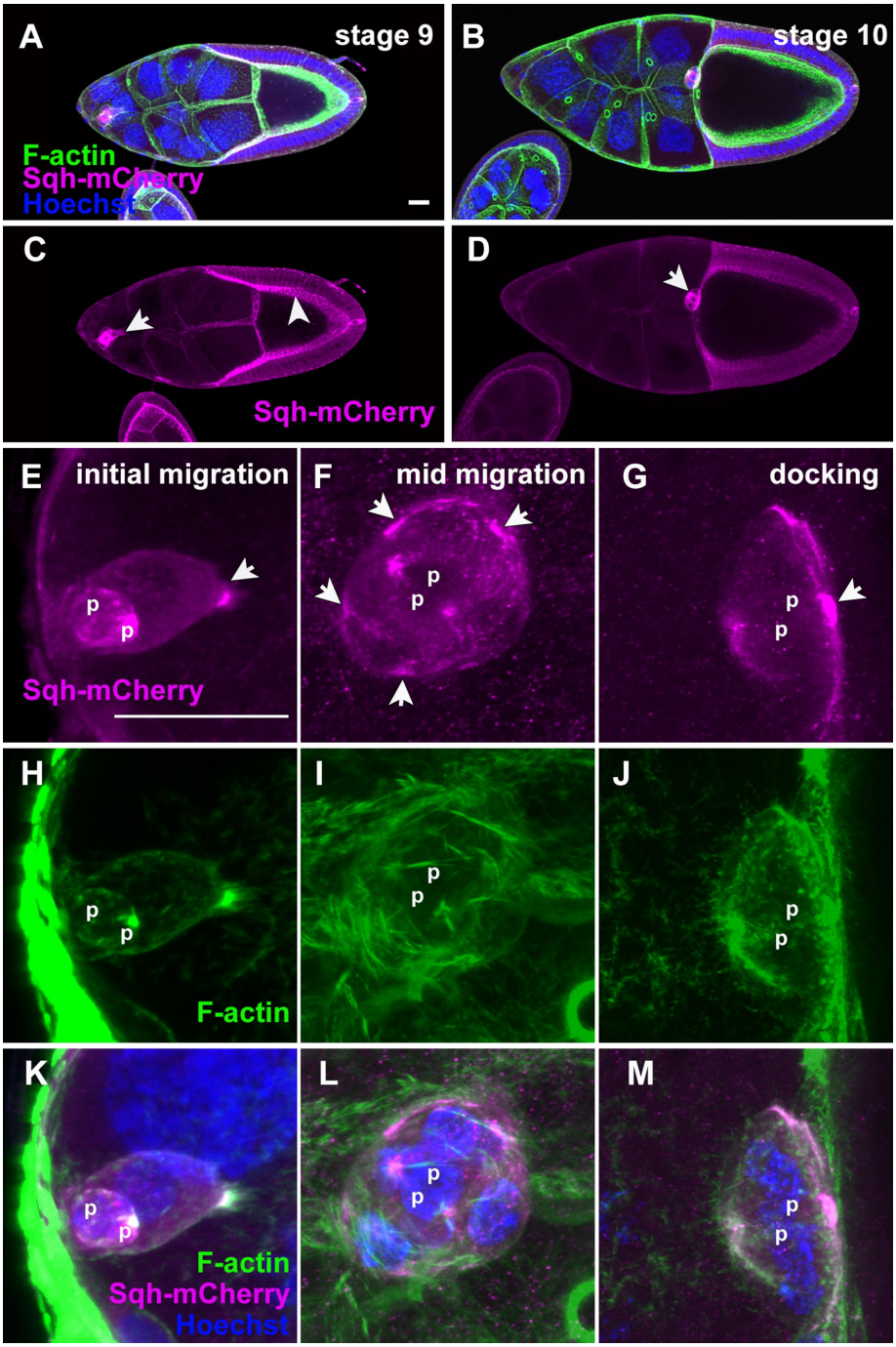

FIGURE 2: Spaghetti squash (sqh) distribution during border cell migration. (A–D) Maximum intensity projections of fixed egg chambers at stages 9 (A, C) and 10 (B, D) labeled with phalloidin for F-actin (green), Hoechst (blue), and expressing Sqh-mCherry expressed from its endogenous promoter and stained using an anti-mCherry antibody. Arrow indicates border cell position and arrowhead indicates apical surfaces of posterior follicle cells (C). (E–M) High-magnification maximum intensity projections of Sqh-mCherry localization during delamination (E, H, K), mid migration (F, I, L), and at the completion of migration (G, J, M). White arrows indicate the accumulation of Sqh-mCherry at the base of protrusions (E), at the cluster periphery (F), and the polar cell (p) apical surfaces facing the oocyte after docking at stage 10 (G). Scale bars in A–D and E-M are same. All scale bars are 20 μm.

(Figure 2E). A similar pattern is observed with a Sqh-GFP and Sqh-TS::GFP (Supplemental Figure S1), although the apical polar cell labeling is more prominent with the mCherry fusion. Knockdown of Sqh by RNAi in polar cells does not result in a detectable phenotype (Majumder *et al.*, 2012), but the Sqh accumulation serves as a useful marker of polar cell position and the apical side of the cluster.

In fixed images of outer, migratory border cells, the pattern of Sqh-mCherry only partially overlaps with F-actin (Figure 2, H–M). The Sqh-mCherry pattern is not identical from one cluster to the other, suggesting it is dynamic. We noted prominent accumulation of Sqh-mCherry at the base of protrusions (Figure 2, E and K). In addition, patches of Sqh-mCherry are evident at the periphery of some clusters during migration (Figure 2, F and L), consistent with a previous report of dynamic Sqh flashes during migration (Aranjuez *et al.*, 2016). At the end of migration, myosin accumulates apically in the cluster at the border cell/oocyte interface (Figure 2, G and M).

To determine to what extent myosin colocalizes with E-cad in migrating border cells, we labeled Sqh-mCherry–expressing clusters with anti–E-cad antibody and imaged them using confocal microscopy. E-cad and Sqh-mCherry colocalized extensively (Figure 3, A–C). Furthermore, Airyscan imaging of fixed samples with amplified GFP and mCherry signals at high lateral and axial resolution revealed a high degree of E-cad and Sqh colocalization at cell–cell junctions within the border cell cluster and the apical surfaces of polar cells (Figure 3, D–I; Supplemental Figure S2).

To compare their dynamics we took z-stacks of Sqh and E-cad for 8 min (Supplemental Movies 2 and 3). To limit phototoxicity, low laser intensities were used, so only the brightest pools of myosin and E-cad were detected (Figure 3, J, K, M, and N). Kymographs from representative clusters show junctional Sqh-mCherry puncta that appear and disappear with a half-life of 30 s (Figure 3L), whereas E-cad is stable for at least 20 min (Figure 3O and unpublished data). Thus, live imaging revealed myosin to be more dynamic than E-cad.

Requirement for myosin II in cell–cell communication

Since Sqh and E-cad colocalize, and E-cad is proposed to mechanically couple border cells, we tested whether myosin also contributes to mechanical coupling. To test the hypothesis that myosin activity mechanically couples lead cells to followers, we inhibited myosin expression or activity in three different ways (Figure 4, A–E). First, we knocked down expression of the light chain using RNAi (Figure 4B). Second, we expressed a nonphosphorylatable form of the light chain (Figure 4C), which likely acts as a dominant-negative (Jordan and Karess, 1997). Finally, we blocked expression of the myosin heavy

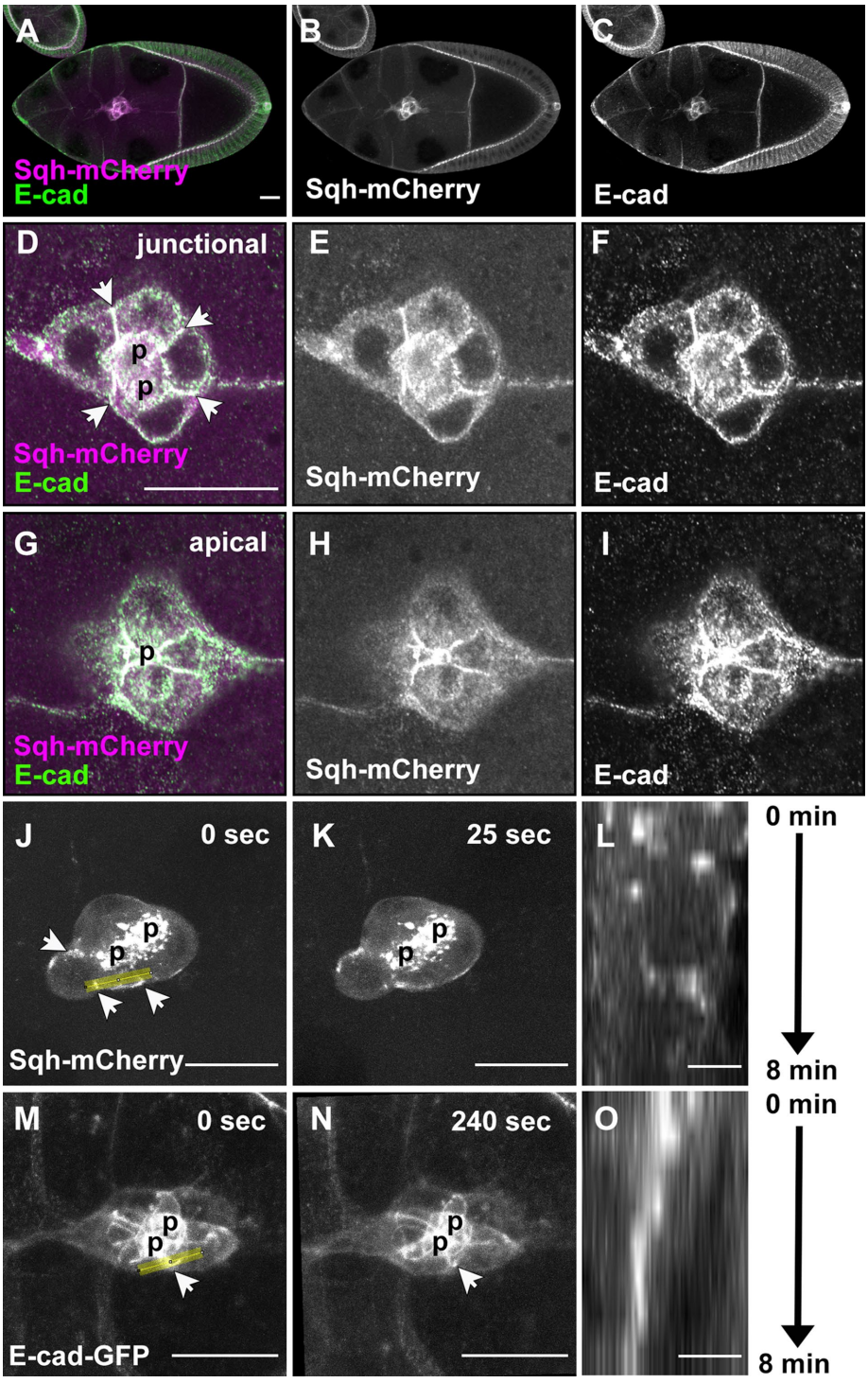

FIGURE 3: Colocalization of Sqh and E-cad during border cell migration. Maximum intensity projections of fixed egg chamber expressing Sqh-mCherry at endogenous levels (labeled by mCherry in magenta) and labeled for E-cad (green) (A–C). (D–I) High-magnification views of single Airyscan slices of fixed border cell clusters at junctional (D–F) and apical (G–I) planes. White arrows mark border cell-border cell junctions. D represents the overlay of E and F. G represents the overlay of H and I. Maximum intensity projections of time-lapse imaging for (J, K) Sqh-mCherry and (M, N) E-cad-GFP. Cell junctions (white arrows) and polar cells (p) are represented. Yellow lines indicate the region used to generate the corresponding kymographs for the duration of movies shown in L and O. Scale bars in A–C, D–I, J and K, M and N, and L, O are same. Scale bars are 20 μm (A–N) and 5 μm (L–O).

chain, known as Zipper (Zip) using RNAi (Figure 4D). Each of these manipulations resulted in a significant fraction of clusters displaying multiple ectopic protrusions (Figure 4E). If myosin-mediated contractility couples the lead cells to the followers, then we would expect that wild-type follower cells in contact with a Sqh-deficient leader would exhibit excess protrusions. To test this, we generated border cell clusters composed of a mixture of wild-type and Sqh RNAi–expressing cells (Figure 4, F–L). Wild-type follower cells indeed exhibited excess protrusions when in contact with Sqh-depleted lead cells (Figure 4, G and L; Supplemental Figure S3; Supplemental Movies S4 and S5). Live imaging of clusters with reduced Sqh showed an overall higher frequency of ectopic side protrusions that are longer lived than those observed in wild-type controls (Supplemental Figure S4; Supplemental Movies S6–S8).

Normally, protrusions from the lead cell (the cell closest to the oocyte) are longer and longer-lived than protrusions from other cells of the cluster (Prasad and Montell, 2007). The small GTPase Rac is essential for border cell protrusion and migration (Murphy and Montell, 1996), and its activity is highest in protruding cells (Wang *et al.*, 2010). Moreover, focal stimulation of a photoactivatable form of Rac (PA-Rac) in one cell is sufficient to steer the entire cluster (Wang *et al.*, 2010). PA-Rac in the lead cell accelerates forward-directed movement, whereas Rac activation in the rear cell reverses the direction of cluster movement (Wang *et al.*, 2010) (Figure 5, A and B). In both cases, Rac activation in one cell stimulates protrusion in the activated cell and inhibits protrusion of other cells (Wang *et al.*, 2010) (Figure 5, A and B). Thus, the protruding cell steers the whole cluster. E-cad is essential for this cell–cell communication (Cai *et al.*, 2014). To test the hypothesis that myosin is similarly required, we expressed PA-Rac together with *sqh* RNAi and photoactivated Rac in the rear cell. Protrusions were defined and quantified as previously described (Wang *et al.*, 2018). Inhibition of Sqh resulted in multiple protrusions, not only in the stimulated cell but also from other cells (Figure 5, C–E). We conclude that the protruding cell inhibits protrusion in following cells in a myosin II-dependent manner. Results were similar for clusters imaged near the beginning of their migration (Figure 5, C–E) or near the end (Supplemental Figure S5).

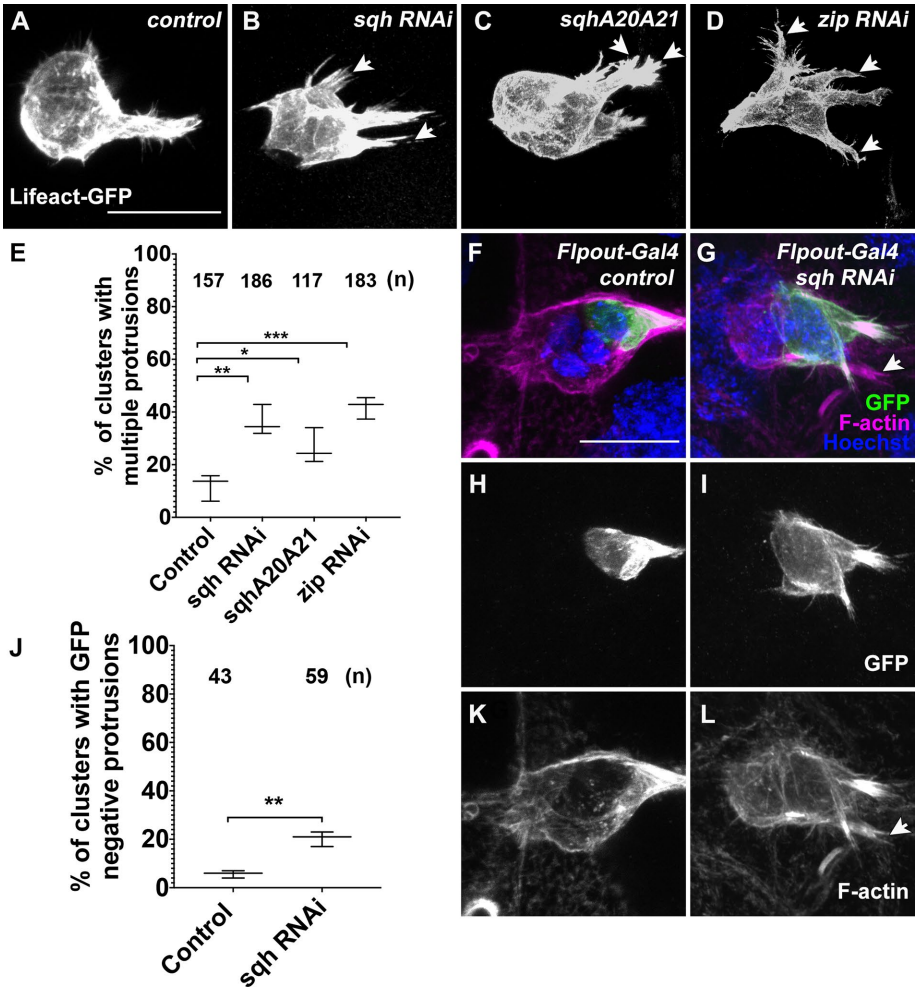

FIGURE 4: Myosin is required for cell communication. (A–D) Fixed imaging of egg chambers stained for *c306-Gal4; tub-GAL80ts* driving *UAS-Lifeact-GFP* together with the indicated *UAS*-transgenes. (E) Box plots of ectopic protrusions in clusters from A–D; (n) represents the total number of clusters counted from at least three independent crosses. Nonautonomous effect of Sqh knockdown on protrusion formation in (F, H, K) control and (G, I, L) *sqh-RNAi* flip-out clones. Clonal region is marked by anti-GFP antibody (H, I) to show autonomous protrusions. Nonautonomous protrusions are shown by F-actin phalloidin staining (white arrows, G, L). (J) Quantification of nonautonomous ectopic protrusions. The *y*-axis indicates percentage of clusters with protrusions in GFP-negative cells; *n* = the number of border cell clusters counted. Statistics represents unpaired *t* test; ***$p < 0.001$, **$p < 0.01$, *$p < 0.05$. Scale bars in A–D and F–L are the same. All scale bars are 20 μm.

To investigate the mechanism of this myosin-mediated protrusion restriction, we evaluated the effects of altering myosin expression or activity on the pattern of Rac activation in border cell clusters (Figure 5, F–L). In wild-type clusters, Rac activity is highest in protrusions (Wang *et al.*, 2010), specifically while they are extending. Lead cell protrusions typically show the highest Rac activity (Figure 5F), whereas nonprotruding clusters do not exhibit higher Rac activity in the lead cell (Figure 5G). To test the effect of myosin on the distribution of Rac activity, we expressed the established Rac FRET probe in border cells together with *sqh* RNAi. Sqh RNAi–expressing clusters showed reduced front enrichment of Rac activity relative to control clusters (Figure 5, H and J). Thus, myosin activity is essential for the asymmetry in Rac activation observed in protruding clusters. Expression of a phosphomimetic version of Sqh (SqhE20E21), designed to cause constitutive activation (Hannaford *et al.*, 2018), had a similar effect (Figure 5, J–L), showing that spatial and/or temporal regulation of myosin activity is essential to establish asymmetric Rac activity.

Myosin distribution depends on E-cad

Since myosin and E-cad colocalize and function in cell–cell communication, we asked whether myosin is recruited in an E-cad–dependent manner. We compared the distribution of Sqh-mCherry in control clusters to those with reduced E-cad expression (Figure 6, A–H). Multiple validated RNAi lines that have varying potencies are available for E-cad (Supplemental Table S1). Since border cells with complete E-cad knockdown rarely migrate (Niewiadomska *et al.*, 1999; Cai *et al.*, 2014), we carried out experiments at low temperature (18°C) that produces a mild migration defect to analyze the effect on myosin. Although this approach risks underestimating the phenotypic effect, we thought it was important to compare migratory control and knockdown clusters rather than compare migratory control clusters to immobile E-cad knockdown clusters. Upon partial E-cad knockdown, we observed both protrusive clusters and rounded clusters, as in controls (Figure 6, A–H; Supplemental Movies S9–S14). Clusters of both morphologies exhibited significantly reduced cortical myosin compared with controls (Figure 6I). To quantify the effect, we used laser scanning confocal imaging to capture time-lapse movies of migrating border cells labeled with Lifeact-GFP and Sqh-mCherry. Using Imaris image analysis software, we segmented the border cell cluster based on the Lifeact-GFP channel and then isolated the cluster perimeter (Supplemental Movie S15). We used the Sqh-mCherry channel to measure cortical myosin levels normalized to the Sqh-mCherry signal in the nurse cells adjacent to the border cell cluster, to correct for photobleaching. Owing to the normal dynamic fluctuations of cortical myosin, there is great variation in the cortical myosin intensity in wild-type clusters (Figure 6I). E-cad knockdown reduced the overall levels and fluctuations of cortical myosin (Figure 6I). Figure 6J illustrates schematically the effects of low versus high cortical myosin both in control and E-cad knockdown clusters. Together these results show that recruitment of myosin requires E-cad–mediated adhesion between border cells.

To assess whether myosin also exerts an effect on E-cad and/or cell–cell contacts, we compared the localization of E-cad in control and *sqh* RNAi–expressing border cells (Figure 6, K–N). We used the FLPout technique (see *Materials and Methods*) so clusters were composed of a mixture of GFP-positive and GFP-negative cells. In control clusters in which both GFP+ and GFP– cells express normal levels of Sqh, E-cad labeling of the apical polar cell domain and border cell/border cell contacts are evident (Figure 6, K and L). In clusters in which the GFP+ cells also express *sqh* RNAi, border cell/border cell contacts appeared irregular in

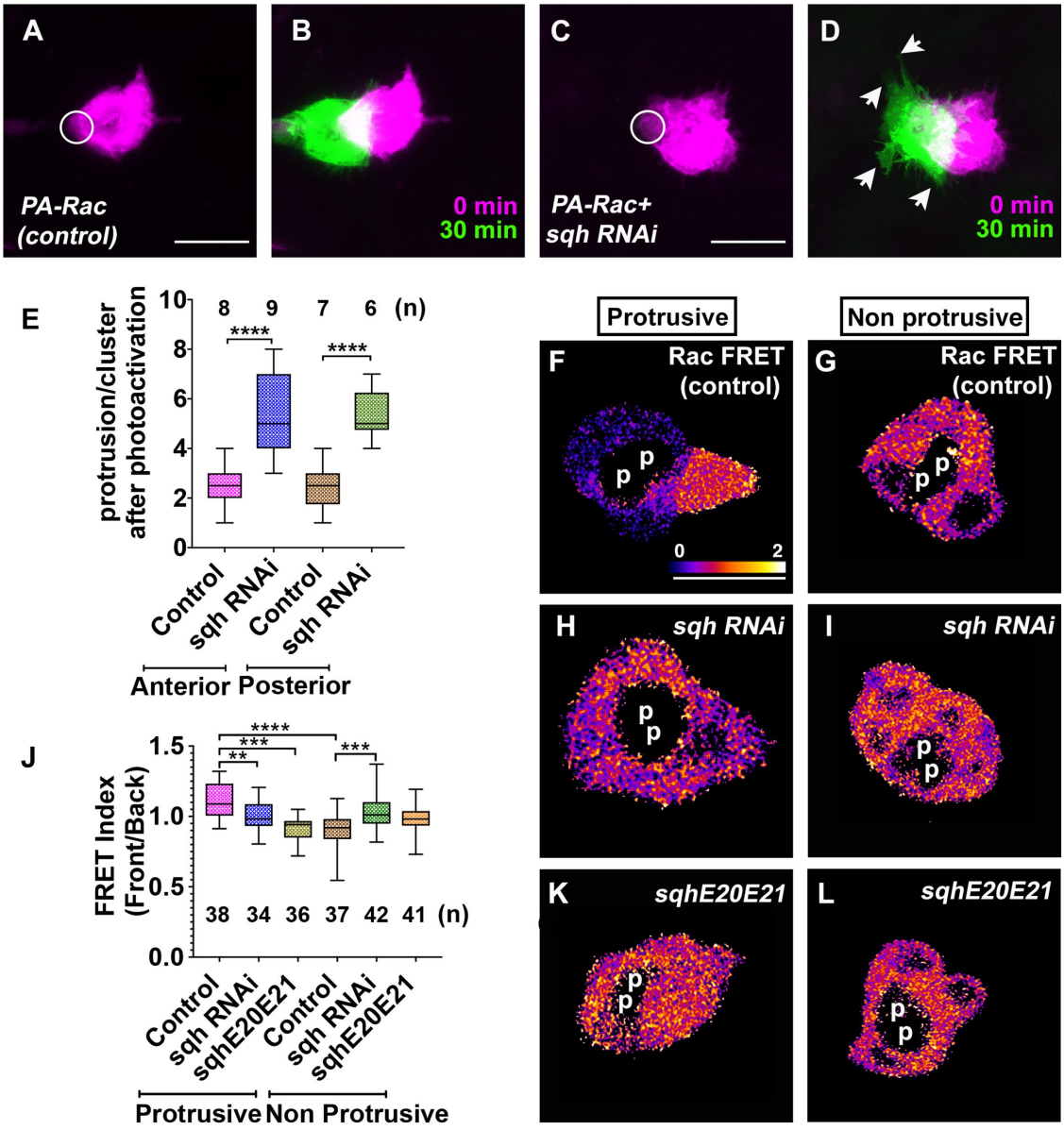

FIGURE 5: Myosin is required for distribution of Rac activity in border cell clusters. (A–D) Live imaging of PA-Rac in *slbo-Gal4* control (A, B) or *UAS-sqh RNAi*–expressing (C, D) clusters. (A ,C) White circle indicates the illuminated region. (B, D) Cluster positions and morphology were marked using mCherry signal in PA-Rac containing flies before (magenta) and after (green) 30 min of photoactivation. White arrows indicate ectopic protrusions. (E) Total number of protrusions observed per cluster for each genotype. Similar results were observed whether clusters were observed near the beginning of migration (Anterior) or near the end (Posterior); (n) indicates the number of clusters evaluated. (F–L) Ratiometric imaging of *slbo-Gal4* driving *UAS-Rac FRET*. Examples of protrusive (F, H, K) or nonprotrusive (G, I, L) clusters are shown. Control clusters expressed *UAS-white RNAi*. Polar cells (p) do not express *slbo-Gal4*. (J) Front/back ratio of measured FRET signals for the indicated genotypes in protrusive and nonprotrusive clusters; (n) indicates the number of clusters imaged. Scale bars in A–D and F–L are same. All scale bars are 20 μm. All data were analyzed by one-way ANOVA with Tukey Kramer post hoc analysis. ****$p < 0.0001$, ***$p < 0.001$, **$p < 0.01$.

8/36 samples examined (Figure 6, M and N) compared with the relatively smooth contacts between control cells in 29/29 clusters (Figure 6, K and L). The remaining 28 *sqh* RNAi samples were not clearly distinguishable from wild type. These results suggest that there is normally actomyosin-mediated tension maintaining border cell-border cell contacts, as in epithelial monolayers in vitro (Warner and Longmore, 2009; Acharya *et al.*, 2018; Charras and Yap, 2018).

Myosin functions in retraction of lead protrusions

We noted prominent but transient accumulation of Sqh-mCherry at the base of protrusions (Figures 2E and 7A; Supplemental Movies S16 and S17), which has not previously been described. We carried out live imaging and found that, as protrusions approach their maximal extension, Sqh-mCherry accumulates and is followed by protrusion retraction. To quantify this effect, we measured the change in protrusion length (ΔL) per unit time (Figure 7B). Positive ΔL indicates

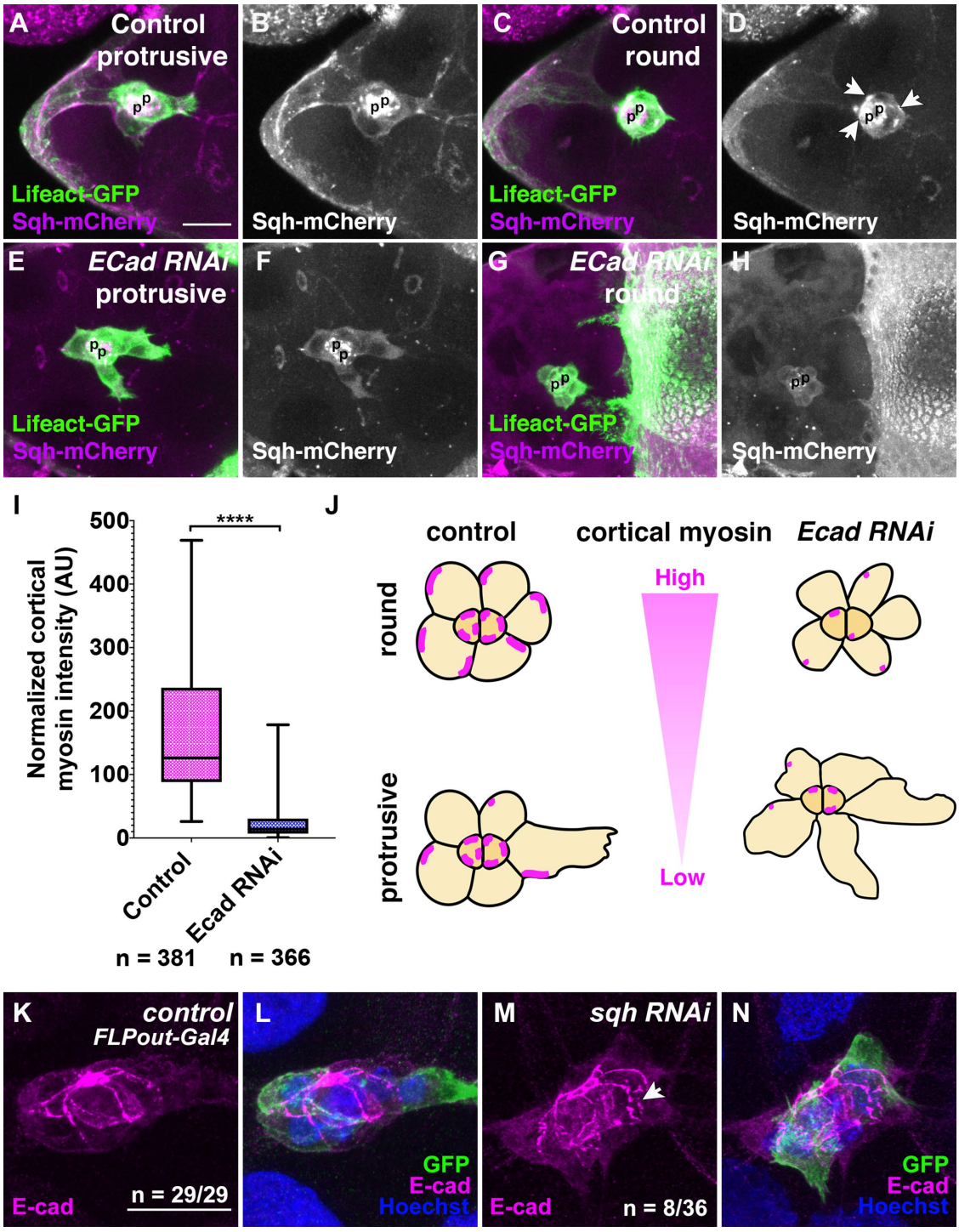

FIGURE 6: Mutual requirement for E-cad and Sqh. (A–H) Stills from time-lapse imaging of clusters coexpressing Lifeact-GFP under the control of the *slbo* enhancer and Sqh-mCherry from its endogenous promoter. (A–D) Control clusters expressing *UAS-white RNAi* in protrusive (A, B) and round (C, D) clusters. (E–H) Border cells expressing *UAS-E-cad RNAi* in protrusive (E, F) and round (G, H) clusters. All genotypes include *c306-Gal4* and were incubated at 18°C. (B, D, F, H) Myosin-only channel. (I) Box plot comparing the average cortical myosin intensity in control vs. *E-cad RNAi*–expressing clusters. n refers to the total number of frames measured from six control and nine *E-cad RNAi* time-lapse movies. (J) Schematic representation of the effects of varying the level of myosin in both protrusive and round clusters. (K–N) Flipout-Gal4–expressing cells (labeled by GFP antibody in green) in clusters expressing control, *UAS-white RNAi* (K, L), or *UAS-sqh RNAi* (M, N) stained for E-cad (magenta). Arrow indicates a discontinuity in the junction as observed in the indicated fraction of clonal clusters. Scale bars in A–H and K–N are the same. All scale bars are 20 μm. Data were analyzed using unpaired *t* test. ****$p < 0.0001$.

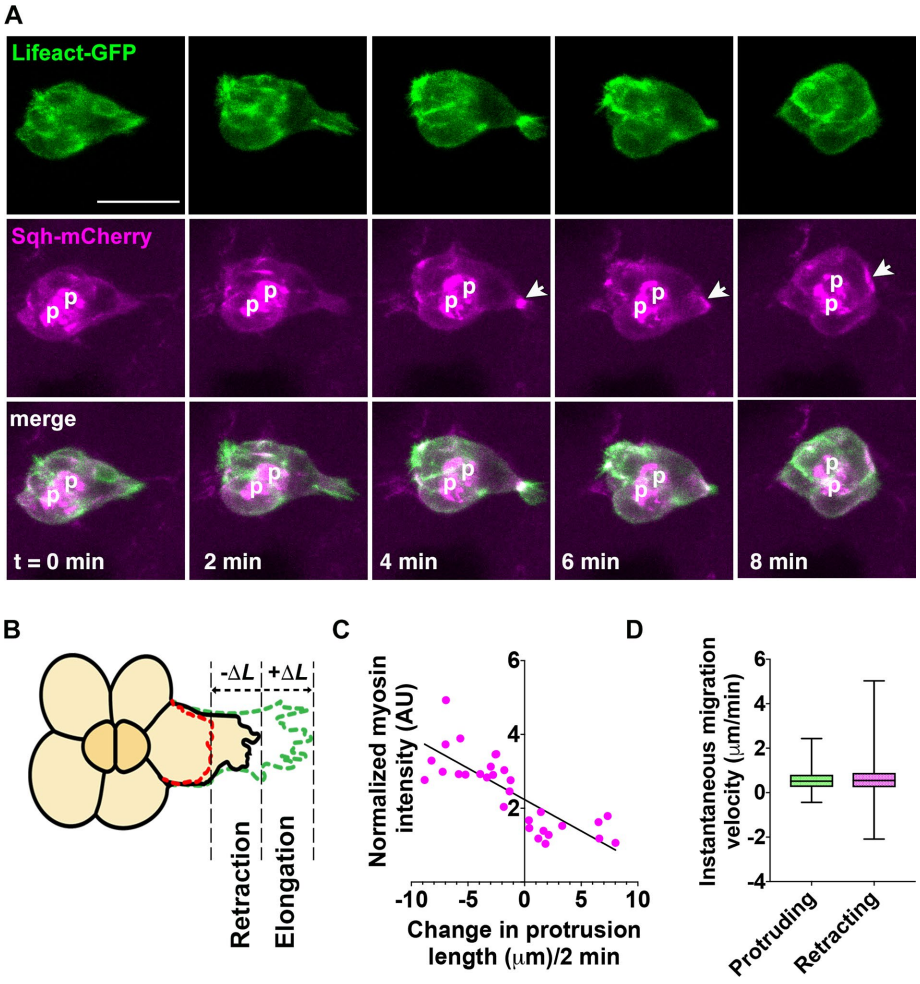

FIGURE 7: Myosin accumulation precedes protrusion retractions. (A) Stills from time-lapse imaging of a representative cluster expressing Lifeact-GFP (green) and Sqh-mCherry (magenta) during one protrusion extension and retraction cycle. Polar cells are marked with p. (B) Schematic showing how changes in lead cell protrusion lengths (ΔL) were measured. (C) Plot of ΔL vs. myosin intensity in 29 protrusion/retraction cycles from three independent time-lapse movies. All scale bars are 20 μm. R^2 value of the trendline is 0.64. (D) Box plot of instantaneous speed from (77) protrusion and (72) retractions cycles.

protrusion while negative values of ΔL represent retraction. Plotting myosin intensity as a function of the rate of change of protrusion length demonstrates a positive correlation between myosin accumulation and retraction and a negative correlation with protrusion (Figure 7C).

This observation forces a reevaluation of the functions of protrusions. On the basis solely of imaging fixed tissue, Fulga and Rørth (2002) suggested that protrusions function as a grapple to pull the cluster forward (Schober and Perrimon, 2002). However such a model implies that the tip of the protrusion adheres strongly to the substrate and would not retract but rather would be subsumed into the advancing cluster. We observed that 130/162 protrusions retracted, suggesting that most protrusions are not effective grapples. The grapple and pull model further predicts that clusters will advance most rapidly when protrusions are maximally extended and that nonprotruding clusters will not advance. We quantified cluster migration speed in relation to protrusion extension and retraction. Importantly, we measured migration speed by following the displacement of the polar cells, rather than following the geometric center of the cluster. This approach is key because the mere extension of a forward-directed protrusion creates an illusion of forward cluster movement when measuring the geometric center, whereas following polar cells does not suffer from this artifact. We found that protruding and retracting clusters move with similar velocities (Figure 7D). Therefore we conclude that protrusions are dynamic and serve some function other than pulling the cluster forward (see *Discussion*).

Phosphomimetic myosin is sufficient to cause a mesenchymal to amoeboid transition in vivo

Tumor cell lines can undergo a transition from mesenchymal to amoeboid migration both in vitro and when xenografted in mice (Pinner and Sahai, 2008; Friedl and Wolf, 2010; Sanz-Moreno *et al.*, 2011). The mesenchymal mode of motility is characterized by high Rac activity and pseudopod-driven movements, similar to normal border cell migration. In contrast, cells that migrate in an amoeboid manner are round and exhibit blebs due to high Rho and Rho kinase activity. Hyperactivation of Rho is sufficient to drive the mesenchymal to amoeboid transition in some cell lines (Panková *et al.*, 2010; Yilmaz and Christofori, 2010). Amoeboid movement is likely dependent on high actomyosin contractility downstream of Rho, however it is unknown whether hyperactivating myosin is sufficient to trigger a mesenchymal to amoeboid transition. Moreover, to our knowledge such transitions have not been reported in untransformed cells.

To test whether constitutive activation of myosin would cause a similar effect, we expressed the phosphomimetic form of Sqh, SqhE20E21. The substitution of glutamate for serine or threonine at these residues mimics the activation by phosphorylation by myosin light chain kinase. We found that SqhE20E2, like active Rho, is sufficient to cause a transition from collective, pseudopod-dependent border cell migration to amoeboid, blebbing motility (Figure 8; Supplemental Movies S6 and S18–S20). Live imaging of SqhE20E21-expressing clusters revealed that in some frames, some cells exhibited small protrusions (Figure 8E and Supplemental Movie S19). This resulted in migration that was slower than control clusters (Figure 8, D and I). Notably, blebbing-based amoeboid motion in SqhE20E21 clusters is faster than protrusive motility (Figure 8, F and I). Even after reaching the oocyte border, cells expressing SqhE20E21 maintain a rounded, blebbing morphology compared with the epithelial morphology of control clusters (Figure 8, G and H). The transition to amoeboid morphology and migration also caused clusters to break into single cells and cell pairs. This suggests that hyperactive actomyosin contractility is sufficient to break the cell–cell adhesions that normally hold the cluster together. Although sqhE20E21 surprisingly displays reduced motor activity in vitro (Vasquez *et al.*, 2016), we observed similar cluster morphology and blebs when we expressed a constitutively active (CA) version of Rho (*Rho1V14*) in

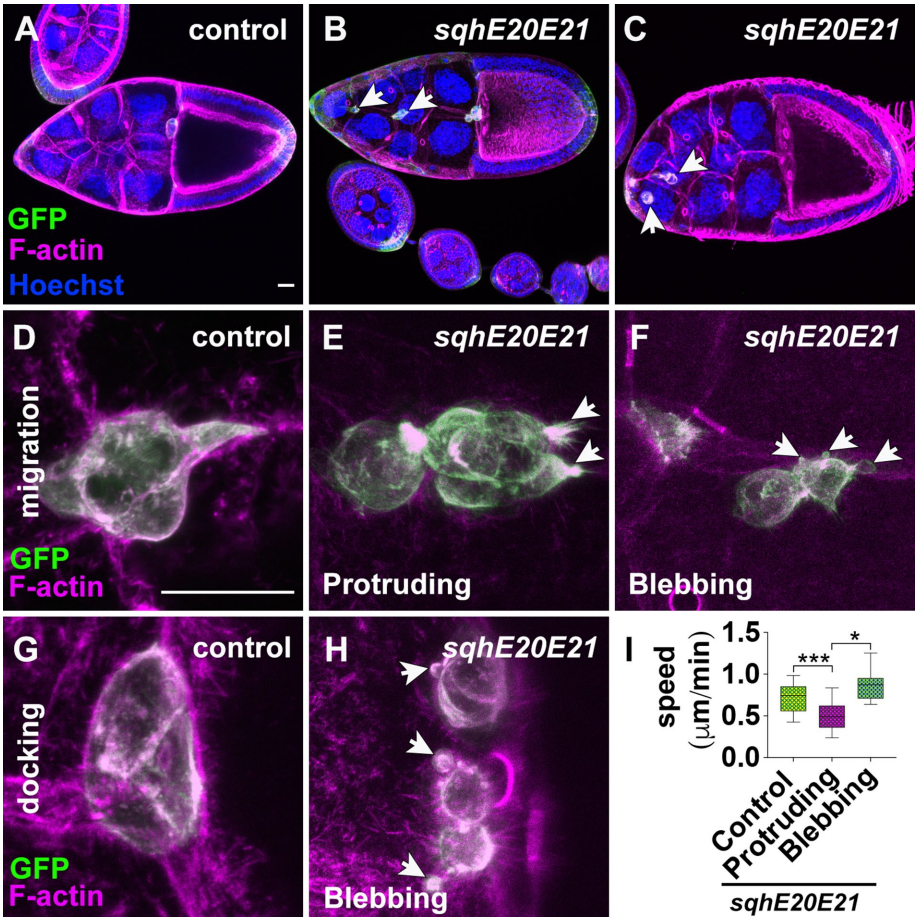

FIGURE 8: Myosin activation causes hypercontractility and membrane blebs. (A–C) Fixed imaging of clusters expressing *c306-Gal4; tub-GAL80ts* driving *UAS-Lifeact-GFP* and *UAS-white RNAi* in control (A), or clusters expressing constitutively active Sqh (B, C). Egg chambers are stained with anti-GFP antibody (green), F-actin (magenta), and Hoechst (blue). Clusters can split and migrate as blebbing amoeboid cells (B) or split into blebbing amoeboid cells that fail to migrate (C). (D–H) High-magnification views of the indicated genotypes in protrusive or blebbing states. Arrows indicate protrusions or membrane blebs in E, F, and H. (I) Box plot of border cell cluster migration speed measured in 10 time-lapses for control and *SqhE20E21* expressing clusters in protrusive or bleb phases. Scale bars in A–C and D–H are the same. All scale bars are 20 μm. All data were analyzed by one-way ANOVA with Tukey Kramer post hoc analysis. ***$p < 0.001$, *$p < 0.05$.

border cells. Thus SqhE20E21 phenocopies hyperactivation of Rho, suggesting that in vivo SqhE20E21 is constitutively active, as expected (Supplemental Movies S21–S22). We conclude that regulation of the level of myosin activity is important because either reducing or increasing activity impaired border cell migration.

DISCUSSION

In this work, we set out to test the hypothesis that myosin mechanically couples border cells at cell–cell junctions in order to communicate direction from leader to follower cells and ended up uncovering diverse and dynamic roles for myosin II within and between collectively migrating border cells. These include both predicted and unexpected functions that lead to a substantial advance in our understanding of the contributions of myosin II to collective, cooperative, cell-on-cell migration in vivo. The results presented here suggest that myosin accumulates and is activated at the base of protrusions where it functions to retract them. Myosin cooperates with E-cad to maintain smooth border cell/border cell contacts, implying that the junctions are normally under tension. Myosin also cooperates with E-cad to communicate direction from the lead cell to followers. The nonautonomous function and the autonomous function within protrusions cooperate to restrict follower cells from protruding. Together with the previously published role for myosin in detachment of the cluster from the anterior, these findings suggest an integrated model (Figure 9).

Rethinking the functions of protrusions

A well-accepted general model for cell motility (Lauffenburger and Horwitz, 1996), based primarily on observations of fibroblast-like cells migrating on hard surfaces in vitro, is that cells protrude via actin polymerization at the front and adhere through nascent adhesions with the substrate, which mature into focal adhesions that anchor F-actin stress fibers. Actomyosin-mediated contraction of the stress fibers then leads to retraction of the cell rear. Some difference between the front and the back must exist so that rear adhesions are preferentially broken. Calpain-mediated cleavage of talin, for example (Cox and Huttenlocher, 1998), specifically at the rear, may account for such differences at least in some cells and circumstances. Quantitative studies of actin dynamics led to a refinement of this model (Ponti *et al.*, 2004). Cells cultured on hard flat surfaces produce a leading lamellipodium composed of treadmilling actin filaments that rapidly polymerize and depolymerize, causing random protrusion and retraction but not substantial adhesion. One to three micrometers behind the leading edge, the lamellum forms where focal adhesions serve as a clutch to anchor F-actin filaments. It is in the lamellum where productive adhesions form, which are necessary for the cell to advance.

It has been unclear how these mechanisms relate to those of cells like border cells that move in three-dimensional environments, surrounded on all sides by pliable matrix or other cells. The shapes of the border cell protrusions are clearly different from the broad and flat lamellipodia and lamella that Ponti studied using speckle microscopy (Ponti *et al.*, 2004). An earlier border cell study based only on fixed tissue analyses proposed a grapple and pull model for initiation of border cell migration by forward-directed protrusions (Fulga and Rørth, 2002). This idea is similar to the original protrusion/adhesion/retraction model for fibroblast migration in vitro (Lauffenburger and Horwitz, 1996). However, the results presented here rule out the grapple and pull model as the major mechanism of forward advancement and suggest an alternative. The grapple and pull model proposes that the border cells extend a long protrusion and grip the substrate at the tip. Then the cell body pulls itself toward the tip, absorbing the protrusion into the cell body in the process. According to such a model, protrusions should not retract and the cluster should reach the furthest extent of each

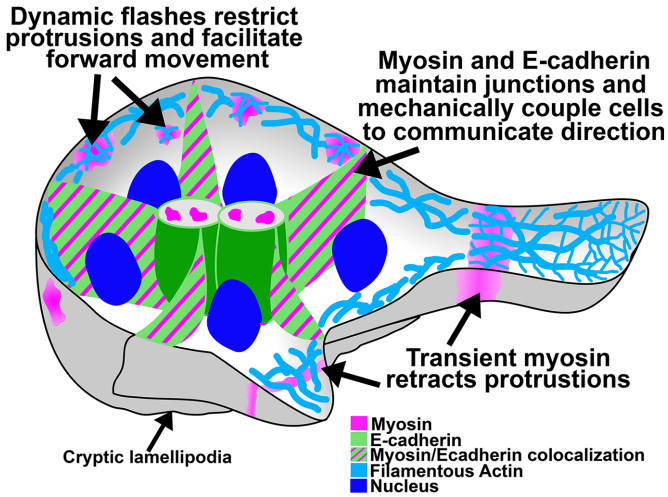

FIGURE 9: Schematic depicting the three localizations and functions of myosin II during border cell migration. These include transient accumulations at the protrusion base that stimulate retraction and inhibit protrusion in nonleader cells. Colocalization with E-cad maintains junctional integrity, and dynamic cortical flashes restrict protrusions from following cells.

protrusion in one step, accelerating as they do. By contrast, the results reported here show that border cells accumulate myosin at the base of a fully extended protrusion and then retract the great majority of protrusions before crawling into the space vacated by them. The cluster continues to crawl forward at a relatively constant speed even as the protrusion retracts. We propose that rather than functioning as a grapple or attachment site, the tip of the protrusion functions as a sensory organ. In this model, protrusions in any direction probe the external environment. Protrusions that encounter a more favorable environment, such as a higher concentration of chemoattractants and/or physical openings, are able to extend further before retracting. Consistent with this idea, all border cells actively crawl to propel the cluster forward. For example, clusters composed of mixtures of wild-type and motility-deficient cells migrate better the more wild-type cells they possess (Silver *et al.*, 2005; Xiang *et al.*, 2016). If only the lead cell pulled the followers forward, one wild-type cell should suffice. Moreover, "cryptic" lamellipodia have been observed in between border cells (Cliffe *et al.*, 2017). These may serve a crawling function similar to the basal protrusions found in all follicle cells at earlier stages, which drive collective migration of the entire epithelium (Barlan *et al.*, 2017).

Similar to the lamellipodium and lamellum described for individual cells migrating on two-dimensional hard surfaces (Ponti *et al.*, 2004), border cells exhibit dynamic protrusion and retraction at the very leading edge. However, the cells are surrounded by other cells and the protrusion is shaped more like a spear than the fan-like lamellipodium/lamellum of single cells migrating unopposed on glass. Nevertheless, though superficially disparate structures, both spear- and fan-shaped protrusions appear to be divided into functionally similar domains of related function: an actin-rich/myosin-poor tip and, a few micrometers further back, a region where actomyosin accumulates and generates contractile force. While we propose that the protrusions probe the microenvironment, productive adhesion between border cells and nurse cells may occur at the base of the protrusion where the actomyosin accumulates, analogous to the lamellum region of a fibroblast. A few differences, in addition to shape, are that the tip of the border cell protrusion must find or make space in between tightly apposed cells, and the whole spear-shaped structure appears and disappears dynamically.

Myosin in cell–cell communication

The observations that myosin colocalizes with E-cad at border cell-border cell contacts, depends on E-cad and is required for communication of direction between the leader cell and followers demonstrate that myosin and E-cad cooperate in collective direction sensing. These findings support the model that mechanical coupling between leaders and followers mediates collective direction sensing (Cai *et al.*, 2014), though the mechanism by which Rac activity and protrusion are inhibited in follower cells remains to be clarified. Since adhesions between collectively invading cancer cells are also under mechanical load (Labernadie *et al.*, 2017), it is likely that the role of myosin II described here also applies in that context.

Peripheral myosin flashes

Aranjuez *et al.* (2016) noted seemingly random flashes of myosin at the border cell periphery and proposed that myosin activity somehow pushes outward to resist inward forces from nurse cells. These authors also proposed that myosin pulls inward to maintain the cluster's rounded morphology. The results presented here are more consistent with the latter idea than the former. The experiments with photoactivatable Rac show that in the absence of myosin, the border cells are capable of extending protrusions in between nurse cells, despite any opposing forces that nurse cells might exert. The myosin knockdown experiments show that myosin normally prevents protrusion in follower cells and mechanically couples leaders and followers to keep all the cells moving in one direction in a coordinated manner. These phenotypes are similar to knockdown of E-cad (Cai *et al.*, 2014, and this study) or of moesin (Ramel *et al.*, 2013), which is an F-actin–binding protein that couples cortical F-actin to the plasma membrane. Together these observations suggest that mechanical coupling between border cells mediated by E-cad and actomyosin coupling keep the cells moving in one direction. The peripheral myosin flashes apparently constrain protrusion, which is consistent with, and a refinement of, the interpretation of Aranjuez *et al.* (2016) that the myosin flashes maintain cluster shape.

Mesenchymal to amoeboid transition in vivo

Cells can migrate using diverse modes (Friedl and Wolf, 2010). They can move as individual cells or as collectives. They can move in a mesenchymal mode or an amoeboid mode. Mesenchymal migration refers to a mode in which cells extend lamellar protrusion and an elongated morphology. They extend protrusions, translocate the cell body, and pull up the rear. In contrast, so-called amoeboid migration is initiated by contraction of the actomyosin cortical cytoskeleton. When the weakest point on the cortex breaks, cytoplasm shoots out forming a bleb. Actin polymerizes into the bleb to stabilize the protrusion and then the rest of the cell moves forward. Transitions between mesenchymal and amoeboid migration have been reported for cancer cells cultured in vitro (Wolf *et al.*, 2003; Wolf and Friedl, 2006; Friedl, 2004; Panková *et al.*, 2010; Yilmaz and Christofori, 2010; Liu *et al.*, 2015). However whether or not normal cells in a native environment can undergo such transitions has been unclear.

Although border cells retain epithelial apical/basal polarity as they move, the protrusion morphologies and Rac-dependence suggest a "mesenchymal-like" mode of migration. The observation that border cells undergo a dramatic transition to amoeboid

migration following expression of a SqhE20E21 establishes that such transitions can occur in normal cells in vivo and that hyperactive myosin in the absence of manipulation of Rho or its downstream kinase Rock is sufficient to drive the transition. The high level of myosin activity also causes the cluster to break apart suggesting that while one level of tension on E-cad junctions is essential to maintain mechanical coupling of the cells, excessive myosin-mediated contraction breaks the cell–cell adhesions. This may be why blebbing-based motility is associated primarily with individually migrating cells such as primordial germ cells (Blaser *et al.*, 2006) rather than collectively migrating cells. These observations suggest that collective, epithelial/mesenchymal border cell migration requires tuning of the magnitudes and vectors of forces generated by Rac, E-cad and myosin. Altering the balance changes their morphologies and behaviors. The distinct morphologies and behaviors of other collectively migrating cells such as the zebrafish lateral line and cranial neural crest may thus emerge from modulating the balance of cadherin-mediated cell–cell adhesion, Rho/Rock/myosin-mediated contractility, and Rac/Cdc42-mediated protrusion.

MATERIALS AND METHODS

Drosophila strains and genetics

The *sqh-mcherry* (59024), *UAS-Rac-FRET* (32050), *UAS-mCherry-PA-RacQ61L* (32049), *UASp-sqh.A20A21* (64114), *UASp-sqh.E20E21* (64411), *E-Cad-GFP* (60584), *slbo-Lifeact-GFP* (58364), *UAS-Rho1V14 (8144),* and *UAS-PLCδ1-PH-GFP (39693)* fly strains used in this study were obtained from the Bloomington Drosophila Stock Center (Bloomington, IN). The *UAS-sqh RNAi* (line 7917), *UAS-zip RNAi* (330299), and *UAS-E-cad RNAi* (103962) were obtained from Vienna *Drosophila* Resource Center (Vienna, Austria). The *sqhAX3; sqh-Sqh:GFP* (III) flies were a gift from Jocelyn McDonald (Kansas State University), and Adam Martin (Massachusetts Institute of Technology) kindly provided *sqh-TS::GFP* lines (Vasquez *et al.*, 2014). The *upd-Gal4,UAS-DsRed.nls* described previously (Xiang *et al.*, 2016) was combined with *slbo-Lifeact-GFP* to perform time-lapse imaging shown in Figure 1, D–I. The *slbo*-Gal4 (Rørth *et al.*, 1998) driver was used to perform all the FRET and photoactivation experiments. The *c306-Gal4; UAS-Lifeact-GFP; tub-GAL80ts* line was combined using *c306*-Gal4 (Manseau *et al.*, 1997) driver with *UAS-Lifeact-GFP* (Cai et al, 2014) and *tub-GAL80ts* (Dai *et al.*, 2017) for RNAi experiments shown in Figures 4, A–D, and 8, A–H, and Supplemental Figure S4, A–L. This driver activates *UAS* transgene expression early in development, allowing time for the RNAi to take effect. The *hsFLP; AyGal4, UAS-GFP* described previously (Xiang *et al.*, 2016) and *hsFLP; AyGal4, UAS-RFP* were used to generate clonal expression of *sqh* in border cells. Desired progeny for live imaging of *sqh RNAi* clones were obtained by crossing *slbo-Lifeact-GFP; UAS-sqh RNAi* to *hsFLP; AyGal4, UAS-RFP* fly stock (Supplemental Figure S3, A–H, and Supplemental Movies S4 and S5).

The *upd-Gal4,UAS-DsRed.nls*, *sqh-mcherry* and *E-Cad-GFP* flies were reared at 25°C and shifted to 29°C for 16–20 h prior to dissection for fixed and live imaging. The *tub-GAL80ts* crosses were set up at 18°C. One-day-old progeny were collected and shifted to 29°C for 3 d before dissection. All the crosses for FRET and photo-manipulation experiments were set at 25°C. One-day-old progeny were collected, transferred on to a dry yeast containing vial, and shifted to 29°C for 16–20 h prior to dissection. For measurement of cortical myosin intensity, control and *E-cad-RNAi* crosses were kept at 18°C to allow partial knockdown of *E-Cad* and border cell movement. For generating *sqh* clones in border cells, flies were heat-shocked twice a day for 1 h, ~4 h apart, in a 37°C water bath. Flies were then kept at 29°C for 3 d prior to dissection.

Immunostaining

Adult female ovaries were dissected in a depression slide containing Schneider's *Drosophila* medium supplemented with 20% fetal bovine serum. Individual ovarioles were pulled out of the muscle sheath using forceps as described (Prasad and Montell, 2007), and mature eggs were discarded. The dissected egg chambers were transferred to a microfuge tube and washed gently with fresh medium. Ovarioles were fixed for 20 min on ice in 4% paraformaldehyde. After fixation, ovarioles were washed with phosphate-buffered saline (PBS) containing 0.4% Triton X-100 (PBST) and incubated with primary antibodies overnight at 4°C. The following primary antibodies from Developmental Studies Hybridoma Bank were used: E-cad (DCAD2, 1:5) and mCherry (3A11, 1:100). Rabbit anti-GFP (G10362, Thermo Fisher) was used in 1:1000 dilution. The next day, ovarioles were washed in PBST and incubated in secondary antibodies for 2 h at room temperature. Alexa Fluor 488– and 568–conjugated secondary antibodies (Thermo Fisher) were used at 1:400 dilution and F-actin was labeled using Phalloidin-Atto 647N (Sigma Aldrich). Samples were washed in PBST and stained with Hoechst (Sigma Aldrich) for 20 min at room temperature. Egg chambers were washed again in PBST and mounted in VECTASHIELD (Vector Laboratories, Burlingame, CA) before imaging.

Airyscan imaging of E-cad and Sqh-mCherry

To observe the colocalization of E-cad and Sqh-mCherry, high resolution airyscan images were collected in Zeiss 800 laser scanning microscope using a 63× Plan-Apochromat (1.4 NA) objective. Images were captured using the Airyscan detector array at 300 nm × 300 nm × 160 nm in the *X*, *Y*, and *Z* dimensions, respectively. Images were Airyscan processed using Zen Blue software (Zeiss).

FRET imaging and analyses

FRET images were obtained from cultured living egg chambers using a Zeiss LSM 780 microscope. A 458-nm laser was used for excitation of the sample. CFP and YFP images were collected simultaneously using channel 1 (464–502 nm) and channel 2 (517–570 nm) under a 40×/1.1 numerical aperture (NA) water immersion objective LD C-Apo lens. Single 16-bit optical sections of frame size 512 × 512 and 3.15 µs pixel dwell in the middle of the cluster were collected each time the cluster makes a protrusion or retracts the forward protrusion. CFP and YFP images were then processed using Fiji image analysis software as described before (Wang *et al.*, 2010). Final YFP/CFP ratio image was generated in Fiji and divided into three equal parts, namely front, middle, and back from the front tip to the rear end of the cluster. The FRET index was calculated as the ratio of front to the back for both protrusive and nonprotrusive clusters. All imaging was performed during the first half of border cell migration.

Photomanipulation of Rac

Photoactivation of Rac and time-lapse imaging were performed using a Zeiss 780 Laser scanning confocal microscope using a 63×, 1.4 NA oil objective lens at 2× zoom. Photoactivation was done at the rear of the cluster in a 8-µm spot using a 458-nm laser set at 5% power with a pixel dwell of 101 µs. The scan was completed in ~ 30 s. Five cycles at 60-s intervals were carried out. Further, z-sections of 1.5 µm thickness spanning the entire border cell cluster were collected using a 568-nm laser. These steps were repeated for an entire time-lapse experiment for a period of 30 min. Maximum intensity projection images before and after photoactivation were generated in Fiji software and the protrusions per cluster after photoactivation were counted using the mCherry signal.

Protrusions were counted using the criteria described in Wang *et al*. (2018.)

Measurement of cortical intensity of myosin

Egg chambers were dissected and mounted as described previously (Prasad and Montell, 2007) and time-lapse imaging was performed using a 40×/1.1 NA water immersion objective. The 1.25-µm-thick z-sections spanning the entire border cell cluster were collected at 150-s intervals using channel 1 (499–553 nm) and channel 2 (570–695 nm) for Lifeact-GFP and Sqh-mCherry, respectively. The z-stack images acquired from time-lapse were then processed in Imaris Image analysis software. Gaussian smooth filter was applied to both channels. Lifeact-GFP channel was used to create a surface and then a mask was applied to collect all Sqh-mCherry signal inside the actin surface. Further, using the cell module in Imaris, a cell of this masked myosin was generated and the surface of this cell was exported for all timepoints. Then, a distance transformation map of this new myosin surface was created for all the inside voxels. A new surface was again created for only the outer 2 µm of cluster periphery. The Sqh-mCherry signal inside the actin surface was then masked to this new surface to obtain only the outer 2-µm signal of Sqh-mCherry. This signal was normalized to the background nurse cell myosin intensity at all timepoints in order to correct for photobleaching effects. See Supplemental Movie S15 for more details.

Measurement of colocalization

Colocalization measurements were done using Fiji image analysis software with the coloc2 plug-in. Analysis was done on all pairwise combinations of E-cad, F-actin, and Sqh-mCherry channels. We report the Pearson correlation coefficient (r) for each of these combinations. The analysis was done in a central z-plane of the border cell cluster as a whole (based on the center of the polar cells), border cell-border cell junctions, and the apical cap of the cluster (as determined by E-cad or myosin signal).

Live imaging of cultured egg chambers for phosphomimetic *sqh*

Dissection and mounting of live egg chambers were performed as described previously (Prasad and Montell, 2007) and time-lapse imaging was performed using a 40×/1.1 NA water immersion objective lens. The 1-µm-thick z-sections ranging the entire border cell cluster were collected at 2-min intervals. Maximum intensity projection was made using the Lifeact-GFP in Fiji image analysis software. Migration speed was calculated for time frames showing either protrusions or bleb-based migration. To calculate the migration speed of these two modes, the displacement of the cluster between the first and last timepoints was divided by the total time elapsed.

Kymograph and myosin intensity during protrusion elongation and retraction

Kymographs for Sqh-mCherry and E-Cad-GFP movies were made in Fiji image analysis software. To quantify myosin intensity during protrusion and retraction, a line scan for the entire protrusion area was drawn using Lifeact-GFP channel to measure the length of protrusion. Myosin intensity was measured in the Sqh-mCherry channel. The average background nurse cell myosin intensity was used to normalize the Sqh-mCherry signal.

Statistical analysis and figure preparation

All statistical analyses (unpaired *t* test and one-way analysis of variance [ANOVA]) and graph preparations were done in GraphPad Prism software. Figures and illustrations were created in Adobe Creative Cloud 2014.

ACKNOWLEDGMENTS

This work was supported by National Institutes of Health grant 5R01GM46425 to D.J.M. and American Cancer Society postdoctoral fellowship PF-17-024-01-CSM to J.P.C.

REFERENCES

Aceto N, Bardia A, Miyamoto DT, Donaldson MC, Wittner BS, Spencer JA, Yu M, Pely A, Engstrom A, Zhu H, *et al*. (2014). Circulating tumor cell clusters are oligoclonal precursors of breast cancer metastasis. Cell 158, 1110–1122.

Acharya BR, Nestor-Bergmann A, Liang X, Gupta S, Duszyc K, Gauquelin E, Gomez GA, Budnar S, Marcq P, Jensen OE, *et al*. (2018). A mechanosensitive RhoA pathway that protects epithelia against acute tensile stress. Dev Cell 47, 439–452.e6.

Aranjuez G, Burtscher A, Sawant K, Majumder P, McDonald JA (2016). Dynamic myosin activation promotes collective morphology and migration by locally balancing oppositional forces from surrounding tissue. Mol Biol Cell 27, 1898–1910.

Barlan K, Cetera M, Horne-Badovinac S (2017). Fat2 and lar define a basally localized planar signaling system controlling collective cell migration. Dev Cell 40, 467–477.e5.

Blaser H, Reichman-Fried M, Castanon I, Dumstrei K, Marlow FL, Kawakami K, Solnica-Krezel L, Heisenberg C-P, Raz E (2006). Migration of zebrafish primordial germ cells: a role for myosin contraction and cytoplasmic flow. Dev Cell 11, 613–627.

Cai D, Chen S-C, Prasad M, He L, Wang X, Choesmel-Cadamuro V, Sawyer JK, Danuser G, Montell DJ (2014). Mechanical feedback through E-cadherin promotes direction sensing during collective cell migration. Cell 157, 1146–1159.

Cai D, Dai W, Prasad M, Luo J, Gov NS, Montell DJ (2016). Modeling and analysis of collective cell migration in an in vivo three-dimensional environment. Proc Natl Acad Sci USA 113, E2134–E2141.

Charras G, Yap AS (2018). Tensile forces and mechanotransduction at cell-cell junctions. Curr Biol 28, R445–R457.

Cheung KJ, Ewald AJ (2014). Illuminating breast cancer invasion: diverse roles for cell-cell interactions. Curr Opin Cell Biol 30, 99–111.

Cheung KJ, Gabrielson E, Werb Z, Ewald AJ (2013). Collective invasion in breast cancer requires a conserved basal epithelial program. Cell 155, 1639–1651.

Cheung KJ, Padmanaban V, Silvestri V, Schipper K, Cohen JD, Fairchild AN, Gorin MA, Verdone JE, Pienta KJ, Bader JS, Ewald AJ (2016). Polyclonal breast cancer metastases arise from collective dissemination of keratin 14-expressing tumor cell clusters. Proc Natl Acad Sci USA 113, E854–E863.

Cliffe A, Doupé DP, Sung H, Lim IKH, Ong KH, Cheng L, Yu W (2017). Quantitative 3D analysis of complex single border cell behaviors in coordinated collective cell migration. Nat Commun 8, 14905.

Cox EA, Huttenlocher A (1998). Regulation of integrin-mediated adhesion during cell migration. Microsc Res Tech 43, 412–419.

Dai W, Peterson A, Kenney T, Burrous H, Montell DJ (2017). Quantitative microscopy of the Drosophila ovary shows multiple niche signals specify progenitor cell fate. Nat Commun 8, 1244.

Ewald AJ, Huebner RJ, Palsdottir H, Lee JK, Perez MJ, Jorgens DM, Tauscher AN, Cheung KJ, Werb Z, Auer M (2012). Mammary collective cell migration involves transient loss of epithelial features and individual cell migration within the epithelium. J Cell Sci 125, 2638–2654.

Friedl P (2004). Prespecification and plasticity: shifting mechanisms of cell migration. Curr Opin Cell Biol 16, 14–23.

Friedl P, Gilmour D (2009). Collective cell migration in morphogenesis, regeneration and cancer. Nat Rev Mol Cell Biol 10, 445–457.

Friedl P, Wolf K (2010). Plasticity of cell migration: a multiscale tuning model. J Cell Biol 188, 11–19.

Fulga TA, Rørth P (2002). Invasive cell migration is initiated by guided growth of long cellular extensions. Nat Cell Biol 4, 715–719.

Hannaford MR, Ramat A, Loyer N, Januschke J (2018). aPKC-mediated displacement and actomyosin-mediated retention polarize Miranda in Drosophila neuroblasts. eLife 7.

Jordan P, Karess R (1997). Myosin light chain-activating phosphorylation sites are required for oogenesis in Drosophila. J Cell Biol 139, 1805–1819.

Labernadie A, Kato T, Brugués A, Serra-Picamal X, Derzsi S, Arwert E, Weston A, González-Tarragó V, Elosegui-Artola A, Albertazzi L, *et al*. (2017). A mechanically active heterotypic E-cadherin/N-cadherin adhesion enables fibroblasts to drive cancer cell invasion. Nat Cell Biol 19, 224–237.

Lauffenburger DA, Horwitz AF (1996). Cell migration: a physically integrated molecular process. Cell 84, 359–369.

Liu Y-J, Le Berre M, Lautenschlaeger F, Maiuri P, Callan-Jones A, Heuzé M, Takaki T, Voituriez R, Piel M (2015). Confinement and low adhesion induce fast amoeboid migration of slow mesenchymal cells. Cell 160, 659–672.

Majumder P, Aranjuez G, Amick J, McDonald JA (2012). Par-1 controls myosin-II activity through myosin phosphatase to regulate border cell migration. Curr Biol 22, 363–372.

Manseau L, Baradaran A, Brower D, Budhu A, Elefant F, Phan H, Philp AV, Yang M, Glover D, Kaiser K, *et al*. (1997). GAL4 enhancer traps expressed in the embryo, larval brain, imaginal discs, and ovary of Drosophila. Dev Dyn 209, 310–322.

Martin AC, Kaschube M, Wieschaus EF (2009). Pulsed contractions of an actin-myosin network drive apical constriction. Nature 457, 495–499.

Montell DJ, Rorth P, Spradling AC (1992). slow border cells, a locus required for a developmentally regulated cell migration during oogenesis, encodes Drosophila C/EBP. Cell 71, 51–62.

Montell DJ, Yoon WH, Starz-Gaiano M (2012). Group choreography: mechanisms orchestrating the collective movement of border cells. Nat Rev Mol Cell Biol 13, 631–645.

Murphy AM, Montell DJ (1996). Cell type-specific roles for Cdc42, Rac, and RhoL in Drosophila oogenesis. J Cell Biol 133, 617–630.

Niewiadomska P, Godt D, Tepass U (1999). DE-cadherin is required for intercellular motility during Drosophila oogenesis. J Cell Biol 144, 533–547.

Onder TT, Gupta PB, Mani SA, Yang J, Lander ES, Weinberg RA (2008). Loss of E-cadherin promotes metastasis via multiple downstream transcriptional pathways. Cancer Res 68, 3645–3654.

Panková K, Rösel D, Novotný M, Brábek J (2010). The molecular mechanisms of transition between mesenchymal and amoeboid invasiveness in tumor cells. Cell Mol Life Sci 67, 63–71.

Pinner S, Sahai E (2008). Imaging amoeboid cancer cell motility in vivo. J Microsc 231, 441–445.

Piotrowski-Daspit AS, Tien J, Nelson CM (2016). Interstitial fluid pressure regulates collective invasion in engineered human breast tumors via Snail, vimentin, and E-cadherin. Integr Biol 8, 319–331.

Ponti A, Machacek M, Gupton SL, Waterman-Storer CM, Danuser G (2004). Two distinct actin networks drive the protrusion of migrating cells. Science 305, 1782–1786.

Prasad M, Montell DJ (2007). Cellular and molecular mechanisms of border cell migration analyzed using time-lapse live-cell imaging. Dev Cell 12, 997–1005.

Rakha EA, Teoh TK, Lee AHS, Nolan CC, Ellis IO, Green AR (2013). Further evidence that E-cadherin is not a tumour suppressor gene in invasive ductal carcinoma of the breast: an immunohistochemical study. Histopathology 62, 695–701.

Ramel D, Wang X, Laflamme C, Montell DJ, Emery G (2013). Rab11 regulates cell-cell communication during collective cell movements. Nat Cell Biol 15, 317–324.

Richardson AM, Havel LS, Koyen AE, Konen JM, Shupe J, Wiles WG 4th, Martin WD, Grossniklaus HE, Sica G, Gilbert-Ross M, Marcus AI (2018). Vimentin is required for lung adenocarcinoma metastasis via heterotypic tumor cell-cancer-associated fibroblast interactions during collective invasion. Clin Cancer Res 24, 420–432.

Rørth P, Szabo K, Bailey A, Laverty T, Rehm J, Rubin GM, Weigmann K, Milán M, Benes V, Ansorge W, Cohen SM (1998). Systematic gain-of-function genetics in Drosophila. Development 125, 1049–1057.

Sanz-Moreno V, Gaggioli C, Yeo M, Albrengues J, Wallberg F, Viros A, Hooper S, Mitter R, Féral CC, Cook M, *et al*. (2011). ROCK and JAK1 signaling cooperate to control actomyosin contractility in tumor cells and stroma. Cancer Cell 20, 229–245.

Schober M, Perrimon N (2002). Unconventional ways to travel. Nat Cell Biol 4, E211–E212.

Shamir ER, Ewald AJ (2015). Adhesion in mammary development: novel roles for E-cadherin in individual and collective cell migration. Curr Top Dev Biol 112, 353–382.

Silver DL, Geisbrecht ER, Montell DJ (2005). Requirement for JAK/STAT signaling throughout border cell migration in Drosophila. Development 132, 3483–3492.

Silver DL, Montell DJ (2001). Paracrine signaling through the JAK/STAT pathway activates invasive behavior of ovarian epithelial cells in Drosophila. Cell 107, 831–841.

Uehara R, Goshima G, Mabuchi I, Vale RD, Spudich JA, Griffis ER (2010). Determinants of myosin II cortical localization during cytokinesis. Curr Biol 20, 1080–1085.

Vasquez CG, Heissler SM, Billington N, Sellers JR, Martin AC (2016). Drosophila non-muscle myosin II motor activity determines the rate of tissue folding. eLife 5, e20828.

Vasquez CG, Tworoger M, Martin AC (2014). Dynamic myosin phosphorylation regulates contractile pulses and tissue integrity during epithelial morphogenesis. J Cell Biol 206, 435–450.

Veracini L, Grall D, Schaub S, Beghelli-de la Forest Divonne S, Etienne-Grimaldi MC, Milano G, Bozec A, Babin E, Sudaka A, Thariat J, Van Obberghen-Schilling E (2015). Elevated Src family kinase activity stabilizes E-cadherin-based junctions and collective movement of head and neck squamous cell carcinomas. Oncotarget 6, 7570–7583.

Wang X, He L, Wu YI, Hahn KM, Montell DJ (2010). Light-mediated activation reveals a key role for Rac in collective guidance of cell movement in vivo. Nat Cell Biol 12, 591–597.

Wang H, Qiu Z, Xu Z, Chen SJ, Luo J, Wang X, Chen J (2018). aPKC is a key polarity determinant in coordinating the function of three distinct cell polarities during collective migration. Development 145, dev158444.

Warner SJ, Longmore GD (2009). Distinct functions for Rho1 in maintaining adherens junctions and apical tension in remodeling epithelia. J Cell Biol 185, 1111–1125.

Wolf K, Friedl P (2006). Molecular mechanisms of cancer cell invasion and plasticity. Br J Dermatol 154(Suppl 1), 11–15.

Wolf K, Mazo I, Leung H, Engelke K, von Andrian UH, Deryugina EI, Strongin AY, Bröcker E-B, Friedl P (2003). Compensation mechanism in tumor cell migration: mesenchymal-amoeboid transition after blocking of pericellular proteolysis. J Cell Biol 160, 267–277.

Xiang W, Zhang D, Montell DJ (2016). Tousled-like kinase regulates cytokine-mediated communication between cooperating cell types during collective border cell migration. Mol Biol Cell 27, 12–19.

Yilmaz M, Christofori G (2010). Mechanisms of motility in metastasizing cells. Mol Cancer Res 8, 629–642.